Journal of Biomedical Optics

SPIEDigitalLibrary.org/jbo

Quantitative microscopy and nanoscopy of sickle red blood cells performed by wide field digital interferometry

Natan T. Shaked
Lisa L. Satterwhite
Marilyn J. Telen
George A. Truskey
Adam Wax

Quantitative microscopy and nanoscopy of sickle red blood cells performed by wide field digital interferometry

Natan T. Shaked,[a] Lisa L. Satterwhite,[a] Marilyn J. Telen,[b] George A. Truskey,[a] and Adam Wax[a]
[a]Duke University, Department of Biomedical Engineering, Fitzpatrick Institute for Photonics, Durham, North Carolina 27708
[b]Duke University Medical Center, Division of Hematology, Department of Medicine, Durham, North Carolina 27708

Abstract. We have applied wide-field digital interferometry (WFDI) to examine the morphology and dynamics of live red blood cells (RBCs) from individuals who suffer from sickle cell anemia (SCA), a genetic disorder that affects the structure and mechanical properties of RBCs. WFDI is a noncontact, label-free optical microscopy approach that can yield quantitative thickness profiles of RBCs and measurements of their membrane fluctuations at the nanometer scale reflecting their stiffness. We find that RBCs from individuals with SCA are significantly stiffer than those from a healthy control. Moreover, we show that the technique is sensitive enough to distinguish classes of RBCs in SCA, including sickle RBCs with apparently normal morphology, compared to the stiffer crescent-shaped sickle RBCs. We expect that this approach will be useful for diagnosis of SCA and for determining efficacy of therapeutic agents. [DOI: 10.1117/1.3556717]

Keywords: red blood cells; erythrocytes; sickle cell disease; sickle cell anemia; cell imaging; quantitative phase microscopy; interferometry.

Paper 11011LR received Jan. 7, 2011; revised manuscript received Jan. 31, 2010; accepted for publication Jan. 31, 2011; published online Mar. 24, 2011.

Sickle cell anemia (SCA) is a recessive genetic blood disorder that is common in people from tropical regions where malaria has been widespread, such as sub-Saharan Africa. SCA is caused by a single-point mutation in the hemoglobin gene, termed hemoglobin S, which leads to polymerization of deoxygenated hemoglobin. Red blood cells (RBCs) of a person with SCA tend to be fragile and less-flexible than normal RBCs. When deoxygenated, sickle RBCs assume a distorted and often crescent shape. RBC abnormalities include deformation, dehydration, and increased adhesivity, which cause multisystem dysfunctions,[1] including vaso-occlusive crisis due to vascular obstruction resulting in ischemia and severe pain, as well as splenic sequestration crisis, aplastic crisis, and haemolytic crisis. Average life expectancy of individuals with SCA is 42–48 years. Changes in mechanical properties of sickle RBCs are attributed to cell wide polymerization of hemoglobin into complex and dynamic fiber systems and to increased association of hemoglobin S with the membrane proteins,[2] among other processes. Improved understanding of the relationship between the physical properties of sickle RBCs and the resulting dynamic behaviors is needed urgently to improve detection, monitoring, and potential treatments for SCA.[3]

Sickle RBCs have been measured by various invasive, contact-based, or force application methods such as micropipette aspiration, cell poking, optical stretching, magnetic twisting cytometry, atomic force microscopy, and optical tweezers.[3–7]

Wide-field digital interferometry (WFDI) is a noncontact technique that is able to record the complex field (amplitude and phase) of the light that has interacted with the sample, where no exogenous labeling or special sample preparation are involved. Using the recorded interference pattern, one can obtain the quantitative phase profile of the sample representing the optical path delay map for each spatial point in the sample image. This map is dependent on both the integral refractive index of the sample and its thickness. We have previously shown that WFDI is applicable for studying cancer cells, chondrocytes, neurons, and cardiomyocytes.[8–13] Mature (enucleated) red blood cells are an attractive goal for WFDI since they can be assumed to have homogeneous refractive index structure and thus RBC thickness profiles can be directly obtained from their quantitative phase profile. WFDI has been used to measure various morphological parameters of RBCs,[14–18] including during malaria.[19]

In this paper, we have applied, for the first time to our knowledge, WFDI techniques to quantitatively image sickle RBCs and to measure the nanometer-scale fluctuations in their thickness as an indication of their stiffness. The technique is capable of simultaneously measuring the fluctuations for multiple spatial points on the RBC and thus can yield a map describing the stiffness of each RBC in the field of view. Using this map, the local rigidity regions of each cell can be quantitatively evaluated. Furthermore, since the technique is basically a quantitative imaging technique rather than one-point measurement, we can use it to simultaneously evaluate cell transverse morphology plus thickness in addition to its stiffness profile. This yields various physical properties for live RBCs in a noninvasive, label-free manner, providing a sensitive tool for diagnosis and research.

WFDI measurements were performed by utilizing an interferometric microscopy setup, reported in detail in our previous publication.[8] In this previous paper, we have used the system for quantitative microscopy of cardiomyocytes, in which thickness and refractive index cannot be easily decoupled. As shown next, this is not the case for RBCs, in which thickness and stiffness measurements can be easily performed by WFDI. In the optical setup, a coherent laser light (17 mW HeNe) is spatially filtered and split to reference and object beams. The object beam is transmitted through the sample and magnified by a microscope objective (40×, 0.66 numerical aperture). The reference beam passes through a similar compensating microscope objective and combined with the object beam at a small angle. A tube lens projects the combined fields on a digital camera (640×480, 7.4 μm×7.4 μm pixels, 120 full frames per second), where an off-axis interferogram of the sample is created. Using a single interferogram, the fully quantitative phase profile of the sample

Address all correspondence to: Natan T. Shaked, Duke University, Department of Biomedical Engineering, Fitzpatrick Institute for Photonics, Durham, North Carolina 27708. Tel: 9196605588; E-mail: natan.shaked@duke.edu.

1083-3668/2011/16(3)/030506/3/$25.00 © 2011 SPIE

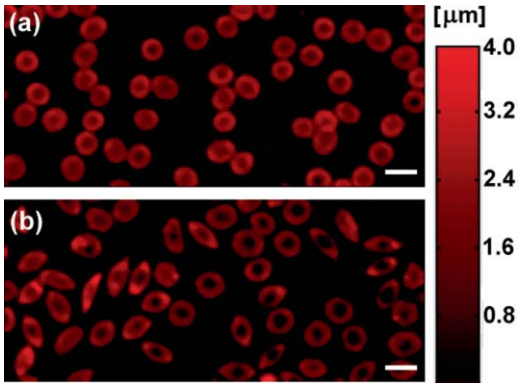

Fig. 1 WFDI thickness profiles of (a) healthy RBCs, (b) sickle RBCs, demonstrating the different RBC morphology that characterizes SCA. Scale bar represents 10 μm. Color bar represents thickness.

is obtained by an improved spatial filtering process that is performed in the image domain,[10,11] followed by a quality-guided phase-unwrapping algorithm. With the presence of a sample containing fluid, the optical path length sensitivity was 4.3 nm.

For the experiments, blood samples were obtained from the Comprehensive Sickle Cell Programs in Duke University and in the University of North Carolina at Chapel Hill and adhered to approved Institutional Review Board protocols. The samples were obtained from two donors with SCA and from a healthy donor. Whole blood was collected in a 4.0 ml K_2EDTA Vacutainer tube (BD367861) or by needle stick and was stored at 4°C. A 50 μl aliquot was washed twice in 1.0 ml Hanks balanced salt solution (HBSS) without calcium, magnesium, or phenol red (Invitrogen/Gibco 14175), and resuspended in endothelial basal media 2 (EBM-2, Lonza) containing 10% fetal bovine serum and growth supplements, which was diluted 2:1 with HBSS. Glass coverslips (22 mm × 50 mm) were treated with 100 μl 1.0 mg/ml poly-D-lysine hydrobromide (SigmaAldrich P7280) in dH_2O for 1 h at 37°C, residual solution aspirated, and 50 μl of the cell suspension allowed to attach for 30 min at 37°C. Attached cells were washed briefly in EBM:HBSS before imaging at 22°C, which was the ambient room temperature. The method is ultimately developed for diagnosis in the field where ambient oxygen pressure and temperature cannot be controlled.

Figure 1(a) presents the quantitative phase profile of the RBCs from a healthy person, demonstrating the characteristic round-biconcave shape which, by allowing an increased surface:volume ratio, facilitates diffusion into and out of the cell and helps deliver oxygen to body tissues, as well as increases cell deformability. The colorbar on the right side of Fig. 1 can be used to interpret the quantitative maps in terms of cell thickness. This interpretation is correct if a constant refractive index can be assumed for the entire cell thickness, which is a valid assumption for healthy RBCs.[14] For sickle RBCs, this assumption is mostly correct, except perhaps in areas where polymerized hemoglobin is present, typically in thin (~20 nm diameter) rod-like fibers spanning the RBCs.[2] In any case, the optical path delay profile can also be directly used to obtain stiffness information, even without calculating the thickness profile.

Figure 1(b) presents the quantitative phase profile of the RBCs from a person, where only a fraction of the RBCs have lost their round-biconcave shape and become crescent shaped.

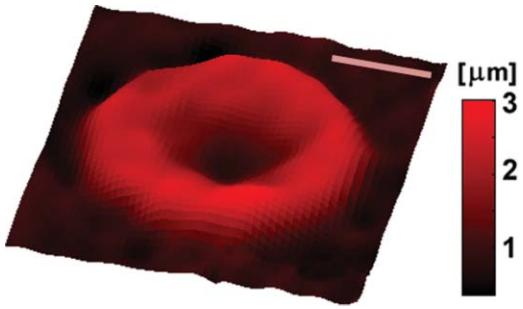

Video 1 WFDI dynamic phase profile of a healthy RBC. Scale bar represents 3 μm. Color bar represents thickness. (QuickTime, 2.2 MB) [URL: http://dx.doi.org/10.1117/1.3556717.1]

We have acquired phase profiles of 24 RBCs obtained from two different persons with SCA and 12 RBCs obtained from a healthy person. For each RBC, phase profiles were collected at a frame rate of 120 frames per second during 10 s and converted into thickness profiles. For each cell, we have calculated the standard deviation of the thickness fluctuations σ_h, which is inversely proportional to the stiffness map of the RBC.[14,15] Averaging σ_h over the entire RBC area, marked as $\langle\sigma_h\rangle$, gives an indication of the cell flexibility, since less rigid RBCs are expected to fluctuate more than stiffer RBCs.

Video 1 presents the dynamic quantitative phase profile and the associated thickness scalebar for one of the analyzed RBCs obtained from the healthy person. This specific cell yielded $\langle\sigma_h\rangle = 64.12$ nm. For comparison, Video 2 presents the dynamic quantitative phase profiles and the associated thickness scalebar of two RBCs obtained from a person with SCA. As can be seen in Video 2, the right cell has a regular round morphology, whereas the left cell has a crescent morphology. These sickle RBCs yielded $\langle\sigma_h\rangle = 28.73$ nm for the round-morphology RBC and $\langle\sigma_h\rangle = 13.54$ nm for the crescent-morphology RBC. Thus, even though the sickle RBC on the right has a visibly normal morphology, it is found to be more than twice as stiff as the healthy RBC.

Figure 2 presents the $\langle\sigma_h\rangle$ values obtained for RBCs of three groups: 12 round-morphology RBCs from a healthy person, 12 round-morphology RBCs from two persons with SCA, and 12 crescent-morphology RBCs from two persons with SCA. Each

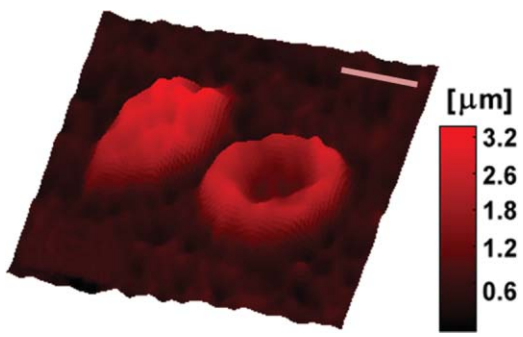

Video 2 WFDI dynamic phase profile of two RBCs obtained from a person with SCA, the right one with round morphology (visibly healthy) and the left one with crescent morphology. The crescent-morphology cell fluctuates less than the round-morphology cell. Scale bar represents 5 μm. Color bar represents thickness. (QuickTime, 2.4 MB) [URL: http://dx.doi.org/10.1117/1.3556717.2]

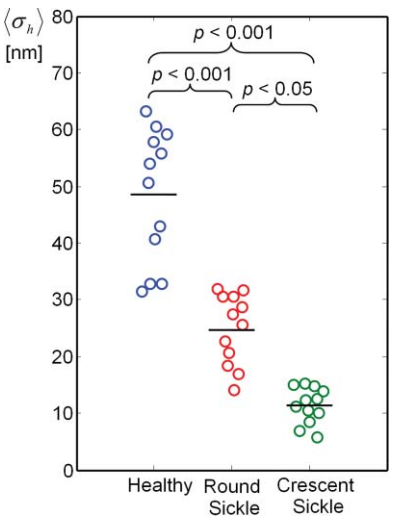

Fig. 2 Standard deviation of RBC thickness fluctuations $\langle\sigma_h\rangle$ averaged over the cell area, obtained from the WFDI dynamic phase profiles of RBCs of three groups: round (typical) morphology RBCs from a healthy person, round (visibly-healthy) morphology RBCs from persons with SCA, and crescent-morphology RBCs from persons with SCA. Each circle represents a different RBC and the horizontal line at each group represents the average value of all cells in the group. *p*-values were calculated by the two-sided Wilcoxon rank-sum test.

of the two groups of 12 sickle RBCs was composed of 5–7 RBCs from the first person with SCA and 5–7 RBCs from the second person with SCA, where no significant difference was seen between the $\langle\sigma_h\rangle$ values of the RBCs from the two individuals with SCA. The healthy RBCs yielded $\langle\sigma_h\rangle = 51.07 \pm 12.02$ nm (which compares favorably with the values obtained for healthy RBCs by Park et al.[15]), the round-morphology RBCs from SCA individuals yielded $\langle\sigma_h\rangle = 21.76 \pm 7.64$nm, and the crescent-morphology RBCs from SCA individuals yielded $\langle\sigma_h\rangle = 13.82 \pm 3.92$ nm. These results demonstrate that the healthy RBCs are two to three times less stiff than the round-morphology sickle RBCs, and the latter are approximately half as stiff as the sickle crescent-morphology RBCs. Greater statistical difference, indicated by the lower *p*-values ($p < 0.001$), is obtained between the group of healthy RBCs and each group of the sickle RBCs than between the two groups of sickle RBCs ($p < 0.05$). The high statistical significance of the difference between the round-morphology RBCs from SCA individuals and the healthy RBCs demonstrates that although the sickle RBC shape might visibly appear to be the same as healthy RBCs, analyzing their thickness fluctuations by WFDI gives a clear indication that they are sickle RBCs.

In summary, we have demonstrated that WFDI is able to obtain dynamic quantitative phase profiles of sickle RBCs in a noncontact noninvasive manner. Based on these profiles, we have calculated the nanometer-scale thickness fluctuations of the RBCs and obtained a metric of their stiffness. Sickle RBCs were found to be significantly stiffer than healthy RBCs. Furthermore, we have demonstrated that it is possible to differentiate between sickle RBC morphologies taken from the same subjects by analyzing their thickness fluctuations, where crescent-morphology RBCs are more rigid (fluctuate less) than round-morphology RBCs. We anticipate that this technique will find uses for diagnosis and monitoring of SCA, as well as usefulness as a research tool, since therapeutic agents that decrease sickling can be expected to improve the abnormal cell rigidity described here.

Acknowledgments

Supported by National Science Foundation (NSF) Grant Nos. CBET-0651622 and MRI-1039562. We thank Dr. Julia Brittain from University of North Carolina for providing us sickle cell anemia blood samples.

References

1. S. K. Ballas, S. Lieff, L. J. Benjamin, C. D. Dampier, M. M. Heeney, C. Hoppe, C. S. Johnson, Z. R. Rogers, K. Smith-Whitley, W. C. Wang, and M. J. Telen, "Definitions of the phenotypic manifestations of sickle cell disease," *Am. J. Hematol.* **85**, 6–13 (2010).
2. L. W. Statius van Eps, "Sickle cell disease," in *Atlas of Diseases of the Kidney*. Vol. 4, R. W. Schrier, Ed., Current Medicine, Inc., Philadelphia, PA (1999).
3. S. Suresh, "Mechanical response of human red blood cells in health and disease: some structure–property–function relationships," *J. Mater. Res.* **21**, 1871–1877 (2006).
4. G. A. Barabino, M. O. Platt, and D. K. Kaul, "Sickle Cell Biomechanics," *Annu. Rev. Biomed. Eng.* **12**, 345–367 (2010).
5. S. K. Ballas and N. Mohandas, "Sickle Red Cell Microrheology and Sickle Blood Rheology," *Microcirculation* **11**, 209–225 (2004).
6. M. M. Brandao, A. Fontes, M. L. Barjas-Castro, L. C. Barbosa, F. F. Costa, C. L. Cesar, and S. T. O. Sead, "Optical tweezers for measuring red blood cell elasticity: Application to the study of drug response in sickle cell disease," *Eur. J. Haematol.* **70**, 207–211 (2003).
7. J. L. Maciaszek and G. Lykotrafitis, "Sickle cell trait human erythrocytes are significantly stiffer than normal," *J. Biomech.* (in press).
8. N. T. Shaked, L. L. Satterwhite, N. Bursac, and A. Wax, "Whole-cell-analysis of live cardiomyocytes using wide-field interferometric phase microscopy," *Biomed. Opt. Express*. **1**, 706–719 (2010).
9. N. T. Shaked, Y. Zhu, N. Badie, N. Bursac, and A. Wax, "Reflective interferometric chamber for quantitative phase imaging of biological sample dynamics," *J. Biomed. Opt.* **15**, 030503 (2010).
10. N. T. Shaked, T. M. Newpher, M. D. Ehlers, and A. Wax, "Parallel on-axis holographic phase microscopy of biological cells and unicellular microorganism dynamics," *Appl. Opt.* **49**, 2872–2878 (2010).
11. N. T. Shaked, J. D. Finan, F. Guilak, and A. Wax, "Quantitative phase microscopy of articular chondrocyte dynamics by wide-field digital interferometry," *J. Biomed. Opt.* **15**, 010505 (2010).
12. N. T. Shaked, Y. Zhu, M. T. Rinehart, and A. Wax, "Two-step-only phase-shifting interferometry with optimized detector bandwidth for microscopy of live cells," *Opt. Express* **17**, 15585–15591 (2009).
13. N. T. Shaked, M. T. Rinehart, and A. Wax, "Dual-interference-channel quantitative-phase microscopy of live cell dynamics," *Opt. Lett.* **34**, 767–769 (2009).
14. G. Popescu, Y. K. Park, W. Choi, R. R. Dasari, M. S. Feld, and K. Badizadegan, "Imaging red blood cell dynamics by quantitative phase microscopy," *Blood Cells Mol. Dis.* **41**, 10–16 (2008).
15. Y. K. Park, C. A. Best, T. Auth, N. S. Gov, S. A. Safran, G. Popescu, and S. Suresh, "Metabolic remodeling of the human red blood cell membrane," *Proc. Natl. Acad. Sci. U.S.A.* **107**, 1289–1294 (2010).
16. B. Rappaz, A. Barbul, Y. Emery, R. Korenstein, C. Depeursinge, P. J. Magistretti, and P. Marquet, "Comparative study of human erythrocytes by digital holographic microscopy, confocal microscopy, and impedance volume analyzer," *Cytometry* **73** A, 895–903 (2008).
17. R. Brazhe, N. A. Brazhe, G. V. Maksimov, P. S. Ignatyev, A. B. Rubin, E. Mosekilde, and O. V. Sosnovtseva, "Phase-modulation laser interference microscopy: an advance in cell imaging and dynamics study," *J. Biomed. Opt.* **13**, 034004 (2008).
18. A. I. Yusipovich, E. Yu. Parshina, N. Yu. Brysgalova, A. R. Brazhe, N. A. Brazhe, A. G. Lomakin, G. G. Levin, and G. V. Maksimov, "Laser interference microscopy in erythrocyte study," *J. Appl. Phys.* **105**, 102037 (2009).
19. Y. K. Park, M. Diez-Silva, G. Popescu, G. Lykorafitis, W. Choi, M. S. Feld, and S. Suresh, "Refractive index maps and membrane dynamics of human red blood cells parasitized by plasmodium falciparum," *Proc. Natl. Acad. Sci. U.S.A.* **105**, 13730–13735 (2008).